

Mechanical and Microstructure Investigation of TiC-inoculated SS316LSi Thin Wall Deposited by CMT-WAAM

Anand Kumar Koppu¹ · Nitin Kumar Lautre¹ ·
Amit Motwani¹ · Yogesh Puri¹

Received: 24 December 2022 / Accepted: 22 March 2023 / Published online: 18 April 2023
© The Indian Institute of Metals - IIM 2023

Abstract Coarse columnar grains are less desired feature of the components manufactured via wire and arc additive manufacturing (WAAM). This can be mitigated by introducing inoculants into melt pool which leads to microstructure grain refinement. In this work, titanium carbide (TiC) nanoparticles of 50 nm average size were added to the molten pool during WAAM of 316LSi stainless steel using cold metal transfer (CMT). The microstructural evolution was studied by optical microscope, scanning electron microscope and X-ray diffraction. The results showed more refined grains for TiC-inoculated specimen due to heterogeneous nucleation promoted by TiC-nanoparticles in the molten pool. Additionally, mechanical tensile testing and hardness profiles were also obtained for the TiC-inoculated and non-inoculated samples. An improvement in the tensile strength and hardness of the TiC-inoculated specimen along with reduction in anisotropy of tensile strength was observed, which could be attributed to the refined grain structure.

Keywords WAAM · CMT · SS316LSi · TiC-inoculants · Grain refinement

1 Introduction

Wire and arc additive manufacturing (WAAM) is classified under direct energy deposition (DED) category of Additive manufacturing (AM) as per ASTM F3187-16 [1]. A high deposition rate of 9.5 kg/h [2] is achieved with WAAM as

compared to laser-based wire AM, where the deposition rate is only 0.7 kg/h [3]. Three thermal energy sources were used for WAAM: Tungsten inert gas (TIG), plasma arc, and metal inert gas (MIG). In comparison with the other two, MIG has the advantage of a coaxial wire feeding system which makes it easier and simpler to deposit layers [4]. However, conventional MIG's limitations include minimum achievable wall thickness and very rough sidewall surface [5]. A modified MIG invention called cold metal transfer (CMT) can help to improve the process-related constraints. The innovative wire retraction mechanism and optimized waveforms in the power source system of CMT allow the droplet transfer in weld pool with minimum heat input [6]. The WAAM process is characterized by high-temperature gradients, high cooling rates and reheating of previously deposited layers which results in non-equilibrium microstructures with coarse columnar grains along build direction in the component. These columnar grains result in hot tearing, solute segregation and anisotropic mechanical properties [7, 8].

AISI 316/316L is common standard grade of austenitic stainless steels. Queguineur et al. [9] demonstrated the possibility to create SS316L filler metal deposition components using WAAM without any significant defects like cracks and internal oxides. Several studies have investigated the effect of various process parameters on the microstructure evolution and their subsequent effect on the mechanical properties of SS316L thin walls [9–12] and blocks [13, 14] fabricated by MIG-WAAM. The methods used to improve the strength of WAAM-deposited components include interlayer hammering [15] and rolling [16]. However, these enhancements are not often available or practical in manufacturing large and complex shapes using the WAAM process. Therefore, an alternate method, such as adding inoculants to the weld pool, can be employed to increase its strength. The use of inoculants to strengthen metal casting components

✉ Anand Kumar Koppu
anandkumarvamsi@gmail.com

¹ Visvesvaraya National Institute of Technology,
Nagpur 440010, India

is common. Inoculants for strengthening components during AM by selective laser melting (SLM) are also reported [17, 18]. Equiaxed grains are challenging to generate in AM processes because of high thermal gradient and fast cooling rates which limit the formation of solutes at the solid/liquid (S/L) interface and consequently restrict heterogeneous nucleation [18]. Therefore, introducing foreign solutes can promote heterogeneous nucleation and the transition of columnar grains to equiaxed grains [7].

Limited studies have investigated the effect of inoculants in the WAAM-deposited steel components. Tiago et al. [19] reported an improvement in strength due to grain refinement by SiC micro-particles (1–2 μm) addition to the molten pool during MIG-WAAM of HSLA steel. Inoculation by micro-particles results in a trade-off between strength and ductility due to large size of the particles and their clusters. This stress concentration increases as the number of particles increases; hence, the addition of appropriate content of nanoparticles will overcome this issue [20]. Zhang et al. [7] reviewed the grain refinement of alloys (Ti, Al, stainless steel, and Ni-based) with inoculants in fusion-based AM and suggested that the role of solute is less important than the role of thermal undercooling and the number density of nucleant particles. Hence, the nanoparticles can be considered as effective nucleants during AM [7]. Researchers [21, 22] have investigated the effect of TiC-inoculants on microstructure and mechanical properties of SS316L manufactured by SLM-AM. It has been reported that TiC-nanoparticles have good wettability because of small contact angle between TiC-nanoparticles and austenitic stainless steel melt during the SLM-AM [18]. To the best of our knowledge, the effect of TiC-nanoparticles on microstructure evolution and mechanical properties of SS316LSi fabricated by WAAM

using CMT has not been reported. In this study, the effects of the trace addition of TiC-nanoparticles during CMT-WAAM of SS316LSi on its microstructure evolution and mechanical properties are examined.

2 Experimental Procedure

Figure 1 shows the experimental setup used for depositing the thin walls. 316LSi filler wire of 1.2 mm diameter was used to deposit the wall on 316L substrate (250 mm \times 50 mm \times 10 mm).

Table 1 displays the chemical composition of the filler wire and substrate. When fabricating the thin wall, two-way depositing strategy was used as recommended by Ortega et al. [23] to minimize geometrical defects. The schematic of the deposition strategy is shown in Fig. 2. Two walls (with and without TiC-inoculants), each of 50 layers with 150 mm length are fabricated using Fronius TPS-400i welding source. In the present study, CMT mode of operation was selected in the welding power source, where it adjusts the current and voltage based on the selected wire feed speed (WFS) via a synergic line.

The process parameters (Table 2) were selected based on the single-layer depositions by varying the WFS and travel speed (TS). In between each deposition layer, TiC-nanoparticles (average size: 50 nm) were added by similar method used by Tiago et al. [19]. Firstly, TiC-nanoparticles were mixed uniformly in ethanol to make TiC alcohol-based suspensions of 3 wt.% concentration and applied with surgical syringe for uniform distribution on deposited layer when the temperature ranged between 150 and 200 $^{\circ}\text{C}$. At this temperature, the ethanol gets evaporated leaving behind

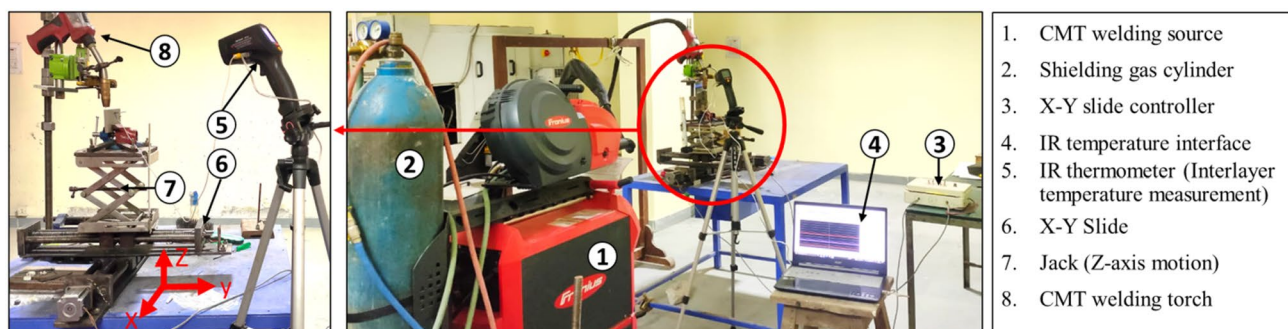


Fig. 1 Experimentation setup

Table 1 Chemical composition of filler wire and substrate

Element	C	Mn	Si	Cr	Ni	Mo	S	P
Filler wire (316LSi)	0.03	1.0–2.5	0.65–1.00	18.0–20.0	11.0–14.0	2.0–3.0	0.03 max	0.03 max
Substrate (316L)	0.02	1.22	0.39	16.82	9.97	2.13	0.09	0.02

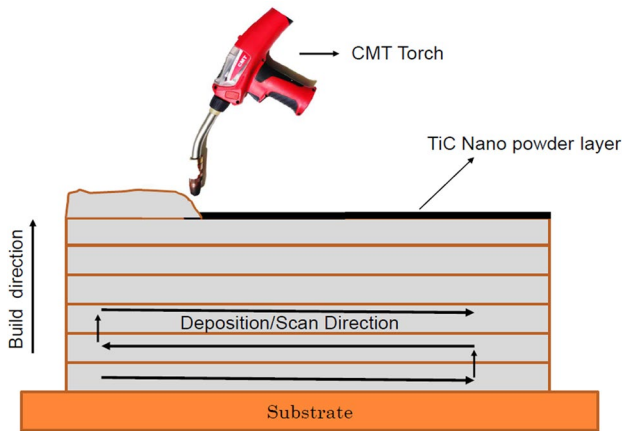


Fig. 2 Schematic showing deposition strategy with TiC addition

Table 2 Process parameters for deposition

Current (A)	Voltage(V)	WFS (m/ min)	TS (mm/s)	Gas flow rate (L/ min)	Shielding gas
150	12.8	5.5	6	15	99.9%Argon

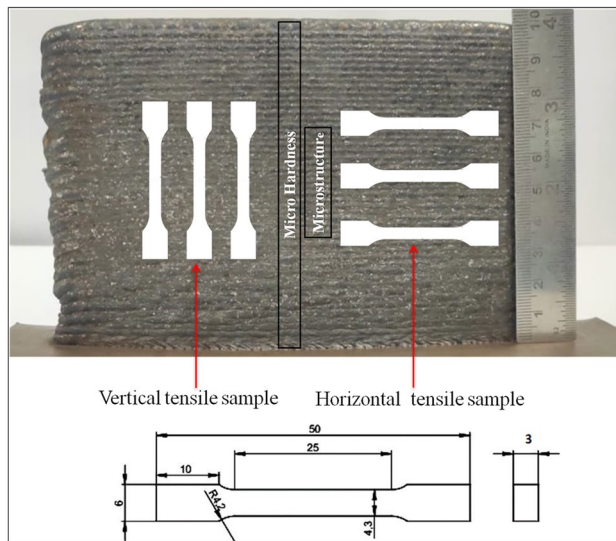


Fig. 3 CMT-WAAM-deposited wall with locations of extracted specimens

the nanoparticles stuck to the layer and these particles are incorporated into the molten pool when the subsequent layer is deposited.

Tensile, microhardness, and metallographic samples are extracted using wire-cut EDM. Figure 3 shows the locations of extracted tensile, microhardness and microstructure specimens from the deposited wall. To observe the

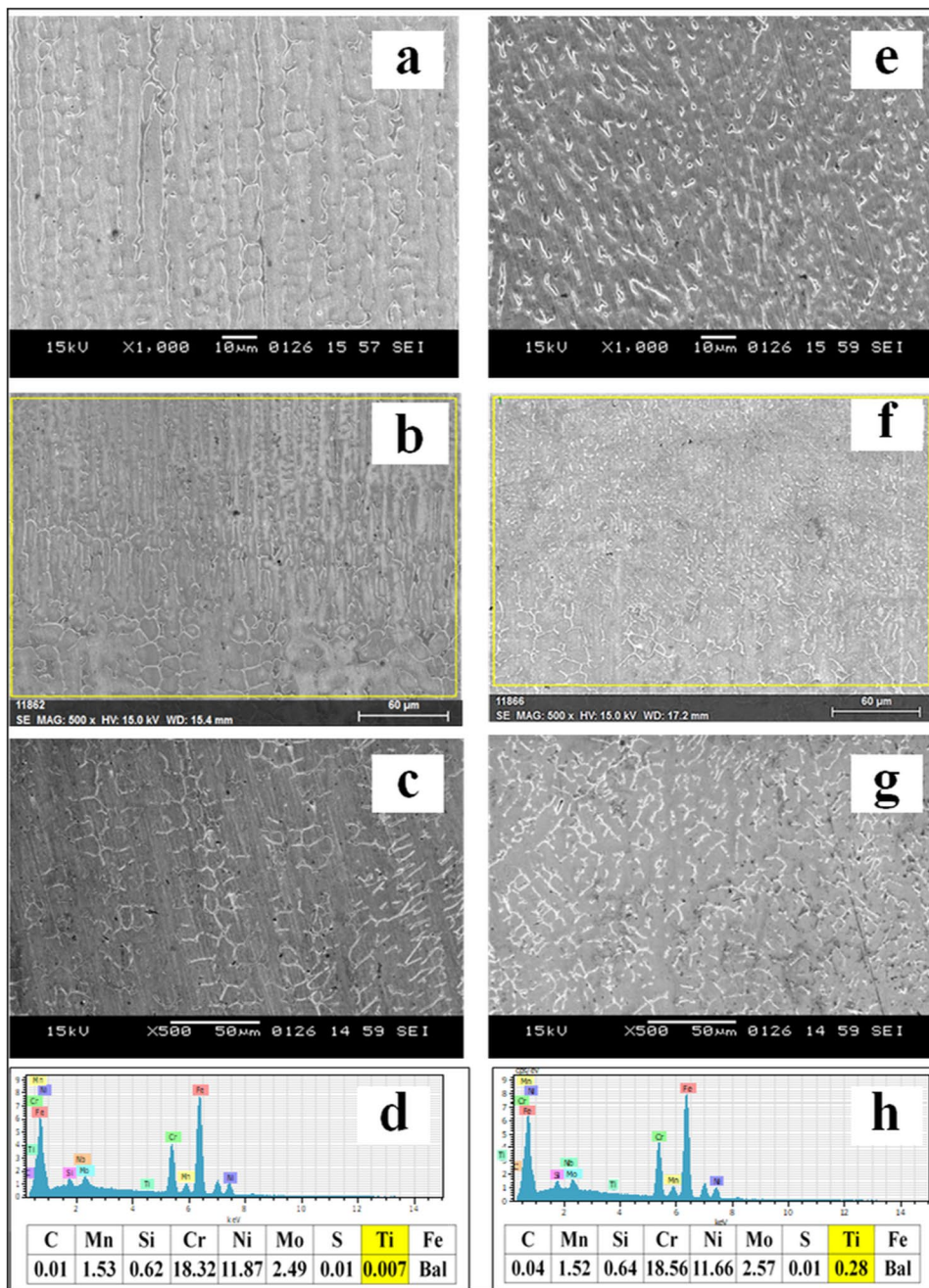
microstructure, transverse section of mid-zone layers sample is taken and polished as per standard metallographic procedures. The microstructure of the cross-sectional surface was explored by optical microscope (Radical make), X-Ray diffraction (XRD) and scanning electron microscope (SEM) (JOEL 6380-A), equipped with energy-dispersive X-ray spectral (EDS) analyzer. Vicker's microhardness was measured by Mitutoyo (HM-12) along the cross section of wall at three zones (bottom, mid and top) with a load of 500 g and dwell time of 15 s. To obtain an average value of the microhardness, the measurement was repeated three times at each zone. Uniaxial tensile tests were performed as per ASTM E8 at the extension rate of 2 mm/s using a UTM (Walter + Bai LFV-250).

3 Results and Discussions

3.1 Microstructure

The content of TiC was estimated using EDS on TiC-inoculated and non-inoculated polished sample. The EDS was performed three times at different locations of each sample, and the identified average chemical compositions of the samples are summarized in Fig. 4d, h. This reveals 0.28 wt.% of Ti, indicating that the introduction of TiC into the molten pool is successful, and Fig. 5 illustrates the Ti elemental mapping. Chemical composition of non-inoculated sample obtained by EDS almost matches with the original wire composition. Figure 6a and b shows the optical micrographs along the transverse section of the non-inoculated and TiC-inoculated fabricated thin wall, respectively, with no porosity or lack of fusion defects. In Fig. 6a-(i) and b-(i), layer fusion boundary above the red dashed-line is visible in a semi-elliptical morphology and it is observed that the dark-colored ferrite (δ) is distributed within the light in color austenite (γ) matrix. In non-inoculated samples, dendritic columnar grains with cellular morphology (Fig. 6a-(ii) and (iv)) without any secondary arms are observed at bottom of the layer just above the fusion boundary and are grown vertically upwards along build direction into coarse columnar grains (Fig. 6a-(iii) and (v)) as observed below the fusion boundary. Similar observations are also found in SEM images in Fig. 4a and c, respectively. These columnar grains are attributed to the large thermal gradient and fast cooling rate which limits the formation of solutes at S/L interface required for heterogeneous nucleation [18]. Whereas, in TiC-inoculated samples (Fig. 6b-(ii) and (iv)) the bottom of the layer, i.e., just above the layer fusion boundary, refined equiaxed cellular grains are observed and in Fig. 6b-(iii) and (v) the top of the layer, i.e., just below the fusion boundary refined dendritic grain structure is observed in which the growth is not in the build

Fig. 4 SEM micrograph with EDS **a, b, c, d** non-inoculated and **e, f, g, h** TiC-inoculated



direction but in random directions. These observations are also found in the SEM images from Fig. 4e to g, respectively.

The reason for a refined dendritic grain structure is due to added TiC-inoculants in molten pool where they acts as a heterogeneous nucleation core, facilitating heterogeneous nucleation during the solidification process and for the similar reason the grains have become random [7]. Grain refinement is achieved when constitutional supercooling surpasses the critical undercooling for nucleation, and the effective heterogeneous nucleation is dependent on sufficient undercooling in conjunction with homogeneous distribution

of potent nucleants particles [24]. A potent inoculant has a little mismatch with the matrix [25]. TiC particles have a small lattice mismatch (14.8%) with the SS316L matrix [18]. The added TiC-nanoparticles reduce the critical nucleation undercooling and will act as potent nucleants for activating the heterogeneous nucleation events during the initial transient stage of solidification [24]. Therefore, a grain refinement effect is observed in TiC-inoculated sample.

Figure 7 shows the XRD results for the non-inoculated and TiC-inoculated sample SS316LSi deposited wall.

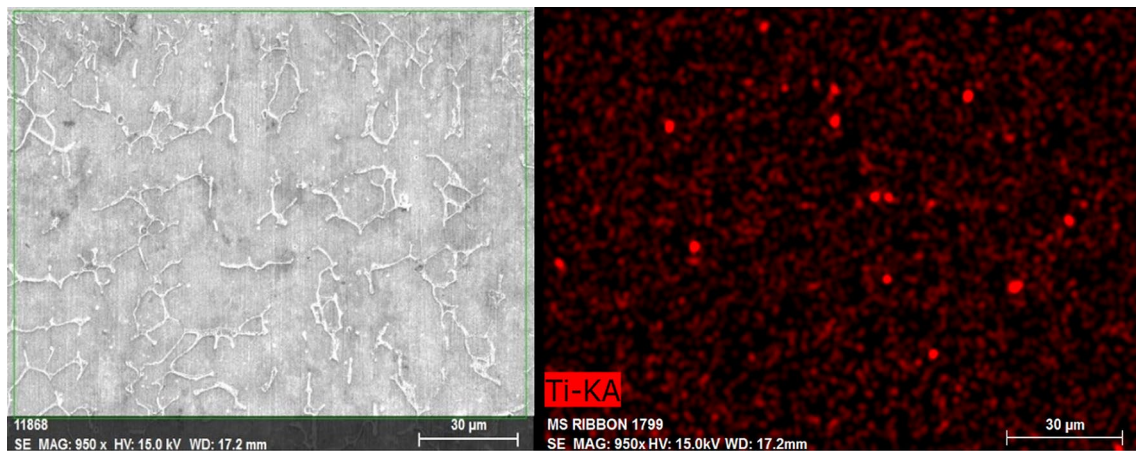


Fig. 5 Ti elemental mapping of TiC-inoculated sample

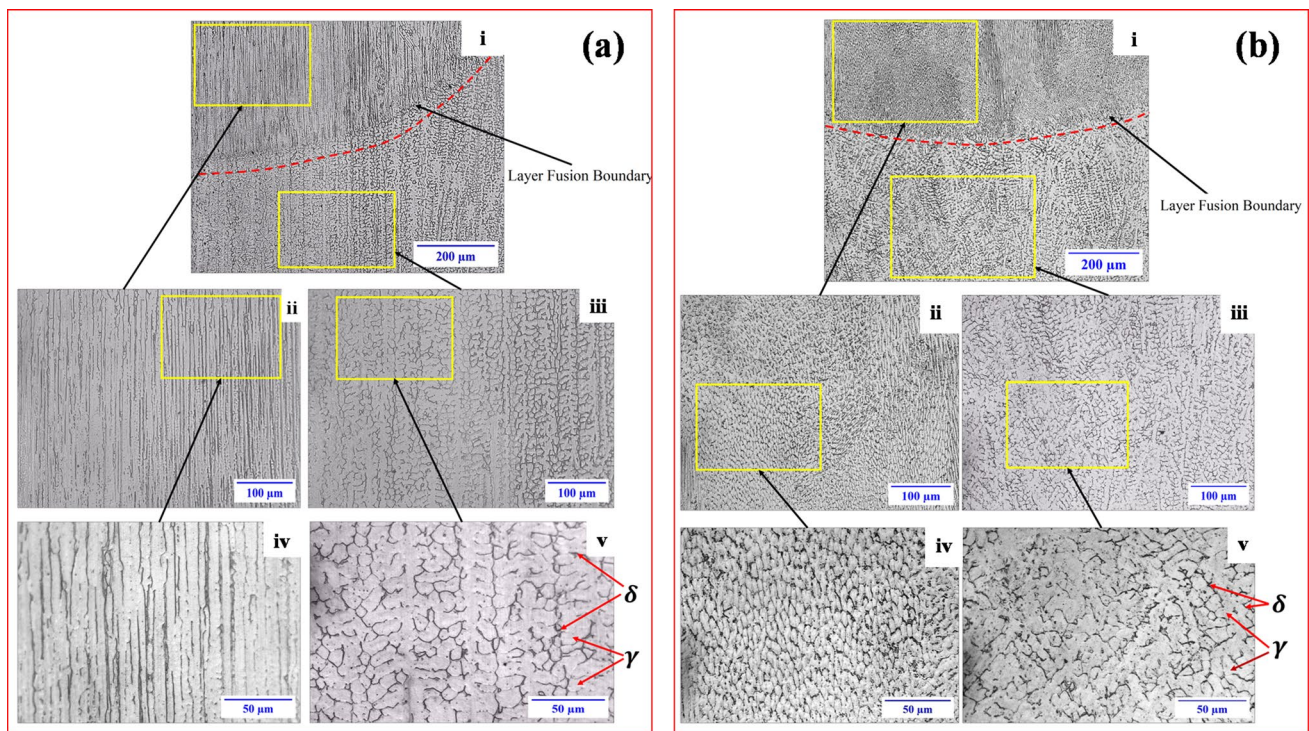


Fig. 6 Optical macrographs **a** non-inoculated **b** TiC-inoculated

Diffraction peaks of austenite (γ) and ferrite (δ) phases are observed from the SS316LSi, and no TiC peaks are observed may be because of its very low content in the component. The austenite (γ) (200) indicates that grain growth is oriented along the build direction, and its peak intensity decreases significantly in the TiC-inoculated sample, indicating that the grain growth orientation along the build direction has decreased to that of the non-inoculated sample.

3.2 Mechanical Properties

3.2.1 Microhardness

Figure 8 shows the microhardness distribution of TiC-inoculated and non-inoculated samples. In non-inoculated samples, the average hardness values are about 169 ± 5.8 HV. A similar trend in the variation of hardness is observed during the deposition of SS316L [26]. While for the TiC-inoculated samples, the average hardness values are about 186 ± 3.6

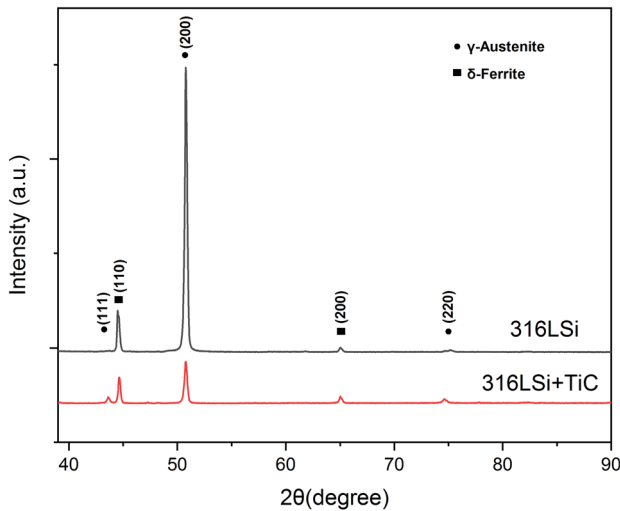


Fig. 7 XRD analysis of non-inoculated and TiC-inoculated sample

HV. The increase in hardness may be attributed to the refined grains obtained by the addition of TiC-nanoparticles. This grain refinement will help in hindering the plastic deformation under load, contributing to increase in microhardness [21]. The added TiC-nanoparticles will uniformly distribute along the grain boundaries which might also contribute to the grain boundary strengthening [27] thereby increasing the microhardness.

3.2.2 Tensile Strength

Figure 9 illustrates the tensile strength properties of TiC-inoculated and non-inoculated samples along the vertical and horizontal orientations. In both TiC-inoculated and non-inoculated samples, the tensile strength along vertical direction is higher than that of horizontal direction. Wu et al. [28] obtained similar trend in his investigation during

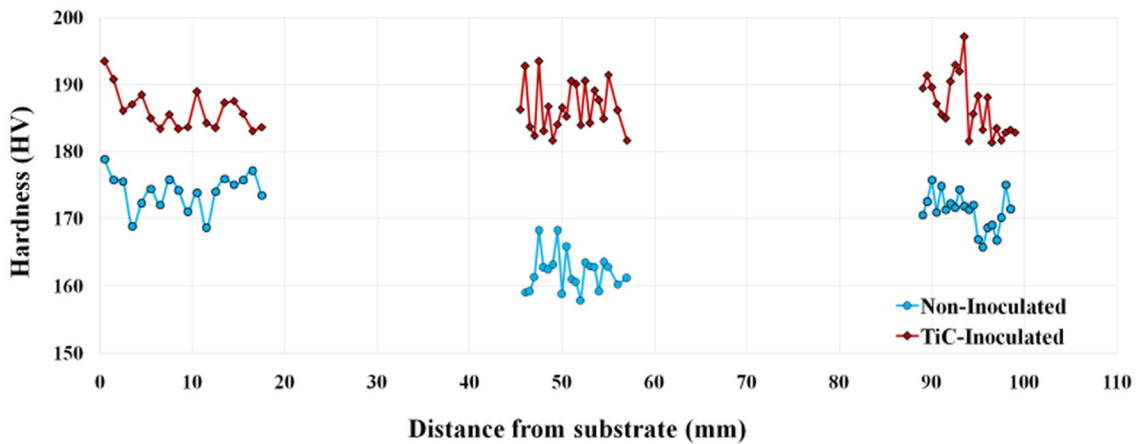


Fig. 8 Microhardness distribution of TiC-inoculated and non-inoculated samples

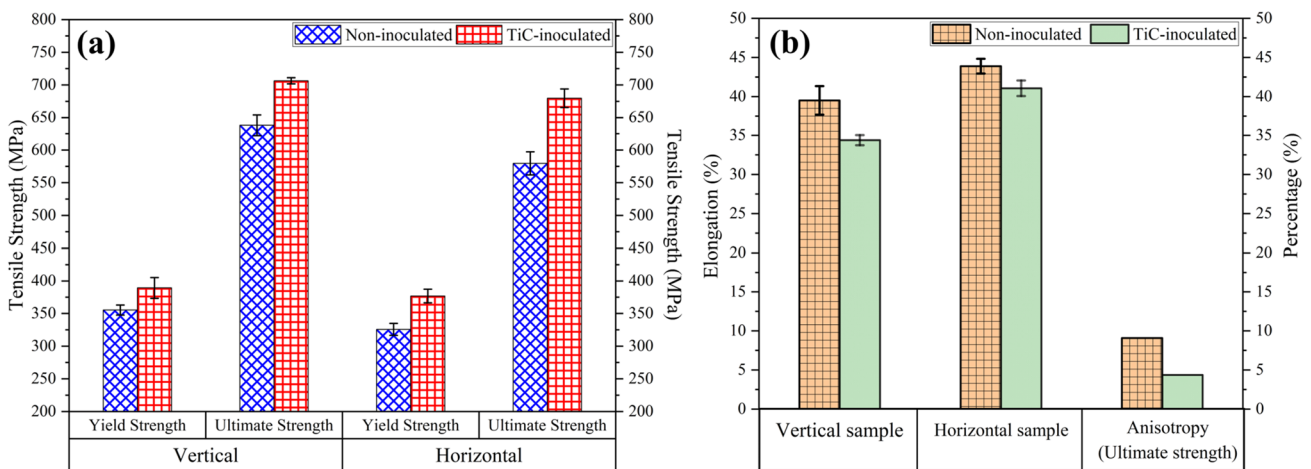


Fig. 9 a Yield and ultimate strength comparison b Elongation and anisotropy comparison

the deposition of SS316L thin wall, where the author analyzed the grain morphology at the fracture and reported that in horizontal tensile stretching, fracture occurred after widening of deformed columnar grains. Whereas, in vertical stretch fracture no grain deformation occurred, and the columnar grain boundaries were the weak link of tensile fatigue. Consequently, tensile strength of horizontal sample with more grain boundaries is low compared to vertical sample.

The average yield strength (YS) and tensile strength (TS) for non-inoculated vertical samples were 355.2 ± 7.7 MPa and 638 ± 16.02 MPa, respectively, while for non-inoculated horizontal samples, they were 325.6 ± 9.1 MPa and 579.6 ± 17.7 MPa, respectively. From Fig. 9a, it can be observed that a significant improvement in YS and TS with the addition of TiC-nanoparticles is achieved. The YS of the TiC-inoculated samples increases to 389.2 ± 16.2 MPa and 376.7 ± 10.4 MPa along vertical and horizontal directions, respectively, when compared to the non-inoculated samples. Similarly, TS of TiC-inoculated is also seen to increase by about 68 MPa and 100 MPa for vertical and horizontal, respectively, in comparison with non-inoculated specimens. According to the Hall–Petch relation, finer microstructure indicates a higher TS [29]. Finer microstructure due to TiC addition increases the count of grain boundaries thus retarding the movement of dislocations under loading.

Table 3 illustrates the comparison of mechanical properties for SS316L manufactured by different methods, and it can be observed that TS of TiC-inoculated SS316LSi of the current study suppresses the other WAAM studies. Increasing wt.% concentration of inoculants in the matrix might improve the strength further [31]. Thus, more study needs to be conducted by increasing the wt.% of nanoparticles and their effect on the mechanical properties. Figure 9b illustrates the elongation to fracture and the percentage of anisotropy of the TiC-inoculated and non-inoculated samples. It can be observed that elongation to fracture of TiC-inoculated samples has decreased to that of non-inoculated samples. The addition of nanoparticles as inoculants in the

molten pool can induce localized embrittlement that results in cracking due to stress concentration when bearing load [32]. Anisotropy of tensile strength is calculated by Eq. 1 [33].

$$\text{Anisotropy} = \frac{P_h - P_v}{P_v} \times 100\% \tag{1}$$

where P_h and P_v represent the average tensile strengths of the horizontal and vertical tensile samples, respectively. It is found that in non-inoculated sample, the anisotropy is about 9% which is reduced to 3.8% after the addition of TiC-nanoparticles. These findings are consistent with microstructure analysis, indicating that anisotropy reduces with the addition of TiC-inoculants. Further research is needed to determine the effect of increasing the wt% of nanoparticles on the microstructure and mechanical characteristics. It is also critical to investigate the influence of TiC-inoculants on corrosion and oxidation resistance of SS316LSi produced by CMT-WAAM. This will be taken into account for future research.

4 Conclusions

In this study, trace addition of TiC-inoculants to the weld pool during CMT-WAAM of SS316LSi and the response on the microstructure evolution and mechanical properties were examined in comparison with non-inoculated CMT-WAAM sample. The key findings were

1. In non-inoculated sample, microstructure evolutions grew from fine dendritic columnar grains to coarse columnar grains along build direction in each layer. After the addition of TiC-inoculants, more refined grains in the sample were observed. XRD analysis also revealed that austenite (γ) (200) peak intensity decreased in TiC-inoculated sample, indicating that grain growth

Table 3 Mechanical properties comparison of SS316L manufactured by different methods

Manufacturing method	Material	TS (MPa)	Elongation (%)	Anisotropy (%)
CMT-WAAM (current study)	SS316LSi	638.0 ± 16.0 (V)	39.5 ± 0.1 (V)	9.09
		579.6 ± 17.7 (H)	43.8 ± 0.9 (H)	
CMT-WAAM (current study)	SS316LSi (TiC- inoculated)	706.4 ± 4.70 (V)	34.4 ± 0.6 (V)	3.8
		679.7 ± 14.3 (H)	41.0 ± 1.0 (H)	
CMT-WAAM [28]	SS316L	550 (V)	–	10
		500 (H)		
GMA-WAAM [30]	SS316L	533 (V)	48	–
SLM [18]	SS316L	722	62 ± 3.1	–
SLM [18]	SS316L (1 wt.% TiC-inoculated)	888	47 ± 0.6	–
Wrought (ASTM)	SS316L	505–578	40	–

orientation along the build direction decreased compared to non-inoculated sample.

2. In non-inoculated sample, hardness distribution was varied along the build direction, and after the addition of the TiC-inoculants, the variation in hardness was reduced. The average hardness increased from 169 ± 5.8 HV up to 186 ± 3.6 HV.
3. Tensile strength of the TiC-inoculated samples was higher compared to the non-inoculated samples, but at the expense of small reduction in ductility. Tensile strength of TiC-inoculated sample increased by about 68 MPa and 100 MPa along the vertical and horizontal, respectively, in comparison with non-inoculated.
4. The anisotropy percentage of tensile strength decreased from 9 to 3.8%. These improvements in hardness, strength and anisotropy in TiC-inoculated samples can be attributed to refined grains.

References

1. ASTM International, Standard Guide for Directed Energy Deposition of Metals. *ASTM Stand.*, p 1, 2016, doi: <https://doi.org/10.1520/F3187>.
2. Martina F, Ding J, Williams S, Caballero A, Pardal G, and Quintino L, *Addit Manuf* **25** (2019) 545. <https://doi.org/10.1016/j.addma.2018.11.022>
3. Baufeld B, Brandl E, and Van Der Biest O, *J Mater Process Technol* **211** (2011) 1146. <https://doi.org/10.1016/j.jmatprotec.2011.01.018>
4. Xu X, Ding J, Ganguly S, Diao C, and Williams S, *J Mater Eng Perform* **28** (2019) 594. <https://doi.org/10.1007/s11665-018-3521-5>
5. Posch G, Chladil K, and Chladil H, *Weld World* **61** (2017) 873. <https://doi.org/10.1007/s40194-017-0474-5>
6. Pickin C G, and Young K, *Sci Technol Weld Join* **11** (2006) 583. <https://doi.org/10.1179/174329306X120886>
7. Zhang D, Prasad A, Bermingham M J, Todaro C J, Benoit M J, Patel M N, Qiu D, StJohn D H, Qian M, and Easton M A, *Metall. Mater. Trans. A* **51** (2020) 4341. <https://doi.org/10.1007/s11661-020-05880-4>
8. Li X, and Tan W, *Comput Mater Sci.* **153** (2018) 159. <https://doi.org/10.1016/j.commatsci.2018.06.019>
9. Queguineur A, Rückert G, Cortial F, and Hascoët J Y, *Weld World* **62** (2018) 259. <https://doi.org/10.1007/s40194-017-0536-8>
10. Wu W, Xue J, and Yao P, *Mater Manuf Process* **35** (2020) 346. <https://doi.org/10.1080/10426914.2020.1726947>
11. Wu W, Xue J, Wang L, Zhang Z, Hu Y, and Dong C, *Metals (Basel)* (2019). <https://doi.org/10.3390/met9010109>
12. Long P, Wen D, Min J, Zheng Z, Li J, and Liu Y, *Materials (Basel)* (2021). <https://doi.org/10.3390/ma14071681>
13. Wang L, Xue J, and Wang Q, *Mater Sci Eng A* **751** (2019) 183. <https://doi.org/10.1016/j.msea.2019.02.078>
14. Wang C, Liu T G, Zhu P, Lu Y H, and Shoji T, *Mater Sci Eng A* (2020). <https://doi.org/10.1016/j.msea.2020.140006>
15. Fang X, Zhang L, Chen G, Huang K, Xue F, Wang L, Zhao J, and Lu B, *Mater. Sci. Eng. A* **800** (2021) 140168. <https://doi.org/10.1016/j.msea.2020.140168>
16. Zhang T, Li H, Gong H, Ding J, Wu Y, Diao C, and Zhang X, *J Mater Process Technol* **299** (2022) 117361. <https://doi.org/10.1016/j.jmatprotec.2021.117361>
17. Zhai W, Zhou W, and Nai S M L, *Mater Sci Eng A* **840** (2022) 142912. <https://doi.org/10.1016/j.msea.2022.142912>
18. Zhai W, Zhou W, and Nai S M L, *Mater Sci Eng A* **832** (2022) 142460. <https://doi.org/10.1016/j.msea.2021.142460>
19. Rodrigues T A, Duarte V R, Tomás D, Avila J A, Escobar J D, Rossinyol E, Schell N, Santos T G, and Oliveira J P, *Addit Manuf* **34** (2020) 101200. <https://doi.org/10.1016/j.addma.2020.101200>
20. Yu W H, Sing S L, Chua C K, Kuo C N, and Tian X L, *Prog Mater Sci* **104** (2019) 330. <https://doi.org/10.1016/j.pmatsci.2019.04.006>
21. Zhao S, Shen X, Yang J, Teng W, and Wang Y, *Opt Laser Technol* **103** (2018) 239. <https://doi.org/10.1016/j.optlastec.2018.01.005>
22. Zhai W, Zhu Z, Zhou W, Nai S M L, and Wei J, *Compos Part B Eng* **199** (2020) 108291. <https://doi.org/10.1016/j.compositesb.2020.108291>
23. Ortega A G, et al., *Sci Technol Weld Join* **24** (2019) 538. <https://doi.org/10.1080/13621718.2018.1564986>
24. Stjohn D H, Qian M, Easton M A, and Cao P, *Acta Mater* **59** (2011) 4907. <https://doi.org/10.1016/j.actamat.2011.04.035>
25. Tan Q, Zhang J, Mo N, Fan Z, Yin Y, Bermingham M, Liu Y, Huang H, and Zhang M X, *Addit. Manuf.* **32** (2020) 101034. <https://doi.org/10.1016/j.addma.2019.101034>
26. Xie B, Xue J, Ren X, Wu W, and Lin Z, *Appl Sci* **10** (2020) 1. <https://doi.org/10.3390/app10093284>
27. AlMangour B, and Grzesiak D, *Mater Des* **104** (2016) 141. <https://doi.org/10.1016/j.matdes.2016.05.018>
28. Wu W, Xu W, Xue J, and Yao P, *Mater Manuf Process* **37** (2022) 1298. <https://doi.org/10.1080/10426914.2021.2006221>
29. Petzh N J, *Nature* **167** (1951) 671. <https://doi.org/10.1038/167671b0>
30. Chen X, Li J, Cheng X, Wang H, and Huang Z, *Mater Sci Eng A* **715** (2018) 307. <https://doi.org/10.1016/j.msea.2017.10.002>
31. Bermingham M, StJohn D, Easton M, Yuan L, and Dargusch M, *Jom* **72** (2020) 1065. <https://doi.org/10.1007/s11837-020-04019-5>
32. AlMangour B, Grzesiak D, Cheng J, and Ertas Y, *J Mater Process Technol* **257** (2018) 288. <https://doi.org/10.1016/j.jmatprotec.2018.01.028>
33. Sun L, Jiang F, Huang R, Yuan D, Guo C, and Wang J, *Mater. Sci. Eng. A* (2020). <https://doi.org/10.1016/j.msea.2020.139514>

Publisher's Note Springer Nature remains neutral with regard to jurisdictional claims in published maps and institutional affiliations.

Springer Nature or its licensor (e.g. a society or other partner) holds exclusive rights to this article under a publishing agreement with the author(s) or other rightsholder(s); author self-archiving of the accepted manuscript version of this article is solely governed by the terms of such publishing agreement and applicable law.